\



Role of compositional changes on thermal, magnetic, and mechanical properties of Fe-P-C-based amorphous alloys

Indah Raya, Supat Chupradit, Mustafa M Kadhim, Mustafa Z Mahmoud, Abduladheem Turki Jalil, Aravindhan Surendar, Sukaina Tuama Ghafel, Yasser Fakri Mustafa, and Alexander N Bochvar

Citation: Chin. Phys. B, 2022, 31 (**1**): 016401. DOI: 10.1088/1674-1056/ac3655
Journal homepage: http://cpb.iphy.ac.cn; http://iopscience.iop.org/cpb

What follows is a list of articles you may be interested in

Internal friction behavior of $Zr_{59}Fe_{18}Al_{10}Ni_{10}Nb_3$ metallic glass under different aging temperatures

Israa Faisal Ghazi, Israa Meften Hashim, Aravindhan Surendar, Nalbiy Salikhovich Tuguz, Aseel M. Aljeboree, Ayad F. Alkaim, and Nisith Geetha

Chin. Phys. B, 2021, 30 (**2**): 026401. DOI: 10.1088/1674-1056/abc14f

Effect of Sn and Al additions on the microstructure and mechanical properties of amorphous Ti-Cu-Zr-Ni alloys

Fu-Chuan Chen(陈福川), Fu-Ping Dai(代富平), Xiao-Yi Yang(杨霄熠), Ying Ruan(阮莹), Bing-Bo Wei(魏炳波)

Chin. Phys. B, 2020, 29 (**6**): 066401. DOI: 10.1088/1674-1056/ab8628

Effect of Ni substitution on the formability and magnetic properties of $Gd_{50}Co_{50}$ amorphous alloy

Ben-Zheng Tang(唐本镇), Xiao-Ping Liu(刘晓萍), Dong-Mei Li(李冬梅), Peng Yu(余鹏), Lei Xia(夏雷)

Chin. Phys. B, 2020, 29 (**5**): 056401. DOI: 10.1088/1674-1056/ab7da8

Secondary relaxation and dynamic heterogeneity in metallic glasses: A brief review

J C Qiao(乔吉超), Q Wang, D Crespo, Y Yang(杨勇), J M Pelletier

Chin. Phys. B, 2017, 26 (**1**): 016402. DOI: 10.1088/1674-1056/26/1/016402

Interstitialcy theory of condensed matter states and its application to non-crystalline metallic materials

V A Khonik

Chin. Phys. B, 2017, 26 (**1**): 016401. DOI: 10.1088/1674-1056/26/1/016401

Role of compositional changes on thermal, magnetic, and mechanical properties of Fe–P–C-based amorphous alloys

Indah Raya[1,†], Supat Chupradit[2], Mustafa M Kadhim[3,4,5], Mustafa Z Mahmoud[6,7], Abduladheem Turki Jalil[8,9], Aravindhan Surendar[10], Sukaina Tuama Ghafel[11], Yasser Fakri Mustafa[12], and Alexander N Bochvar[13,‡]

[1] *Chemistry Department, Faculty of Mathematics and Natural Science, Hasanuddin University, Makassar, South Sulawesi,* 90245, *Indonesia*
[2] *Department of Occupational Therapy, Faculty of Associated Medical Sciences, Chiang Mai University, Chiang Mai,* 50200, *Thailand*
[3] *Department of Dentistry, Kut University College, Kut, Wasit,* 52001, *Iraq*
[4] *College of Technical Engineering, The Islamic University, Najaf, Iraq*
[5] *Department of Pharmacy, Osol Aldeen University College, Baghdad, Iraq*
[6] *Department of Radiology and Medical Imaging, College of Applied Medical Sciences, Prince Sattam Bin Abdulaziz University, Al-Kharj* 11942, *Saudi Arabia*
[7] *Faculty of Health, University of Canberra, Canberra, ACT, Australia*
[8] *Faculty of Biology and Ecology, Yanka Kupala State University of Grodno,* 230023 *Grodno, Belarus*
[9] *College of Technical Engineering, The Islamic University, Najaf, Iraq*
[10] *Department of Pharmacology, Saveetha Dental College and Hospital, Saveetha Institute of Medical and Technical Sciences, Chennai, India*
[11] *Scientific Research Center, Al-Ayen University, Thi-Qar,* 64001, *Iraq*
[12] *Department of Pharmaceutical Chemistry, College of Pharmacy, University of Mosul, Mosul, Iraq*
[13] *Department of Materials Physics, Eotvos Lorand University, Pázmány Péter sétány 1/A, Budapest,* 1117, *Hungary*

(Received 10 May 2021; revised manuscript received 12 August 2021; accepted manuscript online 5 November 2021)

This work aimed to tune the comprehensive properties of Fe–P–C-based amorphous system through investigating the role of microalloying process on the crystallization behavior, glass forming ability (GFA), soft magnetic features, and mechanical properties. Considering minor addition of elements into the system, it was found that the simultaneous microalloying of Ni and Co leads to the highest GFA, which was due to the optimization of compositional heterogeneity and creation of near-eutectic composition. Moreover, the FeCoNiCuPC amorphous alloy exhibited the best anelastic/viscoplastic behavior under the nanoindentation test, which was owing to the intensified structural fluctuations in the system. However, the improved plasticity by the extra Cu addition comes at the expense of magnetic properties, so that the saturation magnetization of this alloying system is significantly decreased compared to the FeCoPC amorphous alloy with the highest soft magnetic properties. In total, the results indicated that a combination of added elemental constitutes, *i.e.*, $Fe_{69}Co_5Ni_5Cu_1P_{13}C_7$ composition, provides an optimized state for the comprehensive properties in the alloying system.

Keywords: Fe-based alloy, saturation magnetization, glass forming ability, viscoplastic

PACS: 64.70.pe, 65.60.+a, 71.55.Jv, 75.50.Kj **DOI:** 10.1088/1674-1056/ac3655

1. Introduction

In recent years, Fe–P–C-based alloying system has received significant attentions for developing Fe-based alloys with great soft magnetic features such as low coercivity and high permeability.[1–3] Moreover, due to their low-cost production, Fe–P–C-based alloys have been identified as promising materials for commercial applications.[4,5] Nevertheless, the undesirable glass forming ability (GFA) and relatively low saturation magnetization are main challenges for their extensive use in energy-conversion devices.[6,7] To tackle these problems, repeated attempts have been made to improve the GFA and saturation magnetization simultaneously.[8–10] Several investigations have shown that the late transition metals (LTMs) and metalloids (M) are suitable microalloying elements for enhancing the GFA and soft magnetic properties. Whereas, the GFA improvement by transition metals (TMs) comes at the expense of saturation magnetization.[11–14] To provide some examples, Li *et al.*[15] fabricated $Fe_{81}P_{8.5}C_{5.5}B_2Si_3$ amorphous alloy with critical diameter of 1 mm and a saturation magnetization (J_s) of 1.56 T, which was suitable for the commercial applications. Yang *et al.*[16] produced FeCuPC alloys by fluxing treatment and *J*-quenching technique. They indicated that the Cu addition increases the yield strength and plasticity of $Fe_{79.4}Cu_{0.6}P_{13}C_7$ nanocomposite and keeps J_s around 1.5 T. Hou *et al.*[17] reported that the substitution of B for P essentially improves the saturation magnetic flux density (B_s) of FePBCCu amorphous alloys. Using synchrotron x-ray diffraction (XRD), it was also found that the rise of P/C ratio increases the average atomic volume and Fe–Fe pairs in the Fe–P–C alloying system.[18] In another study, it was reported that the P increment in the Fe–P–B–C alloying composition leads to a brittle-to-ductile

†Corresponding author. E-mail: indahraya@unhas.ac.id
‡Corresponding author. E-mail: Alexander.Bochvar1985@gmail.com

© 2022 Chinese Physical Society and IOP Publishing Ltd

transition.[19] Based on another work, it was revealed that the Mo addition in the Fe–P–C system improves the GFA and strength.[20] Ma *et al.*[21] indicated that the minor Ni addition in the Fe–P–C system significantly enhances the GFA and makes an optimum alloying composition for the Curie temperature. However, the extra Ni addition leads to decrease of the J_s value. Other investigations also confirmed that the Ni addition just has positive effects on the glass formation of Fe-based systems.[22,23] In several studies, it was showed that Co element is also suitable for improving GFA and plasticity of Fe–P–C alloy and creates an optimized J_s in the range of 1.5 T–1.6 T.[24,25]

As aforementioned, there are several investigations focusing on the effects of added elements into the Fe–P–C alloys. However, few works have been done to systematically show the effects of multiple microalloying elements on the final properties. Moreover, tuning the comprehensive properties of Fe–P–C alloy is still one of the most heated debates.[26–30] Therefore, we made an effort to design and fabricate alloying compositions based on Fe–P–C system and optimize the mentioned properties to achieve an Fe-based amorphous alloy for the promising applications. To reach this goal, several elemental constitutes with different atomic features were picked out to add into the Fe–P–C system, somehow to improve the comprehensive properties.

2. Materials and methods

Pure elements comprising Fe, Ni, and Co along with high purity graphite (99.98%) and FeP pre-alloy were used to produce the ingots by arc re-melting process under pure Ar environment. The prepared ingots were re-melted four times to obtain the homogenous alloying compositions. The final compositions were $Fe_{80}P_{13}C_7$, $Fe_{75}Ni_5P_{13}C_7$, $Fe_{75}Co_5P_{13}C_7$, $Fe_{70}Co_5Ni_5P_{13}C_7$, $Fe_{69}Co_5Ni_5Cu_1P_{13}C_7$, and $Fe_{65}Co_5Ni_5Cu_5P_{13}C_7$ hereafter called as S1, S2, S3, S4, S5, and S6 respectively. Using machine learning algorithm proposed in Ref. [31], we were sure of the glass formation of alloying compositions. After the primary processes, the melt spinning technique was applied to fabricate amorphous ribbons with 40-μm thickness and 3-mm width. The x-ray diffraction (XRD Co-$K\alpha$) experiment was carried out to confirm the amorphous nature of ribbons (see Fig. 1). The differential scanning calorimetry (DSC-Perkin Elmer 8000) was conducted to study the thermal characteristics of samples in a wide range of temperatures. The test was conducted under the high-purity Ar environment and 20-K/min heating rate. The room-temperature J_s values (M–H hysteresis curves) of specimens were attained using a quantum design physical property measurement system with vibrating sample magnetometer (VSM) option. The microstructure of MGs was analyzed through the high resolution transmission electron microscopy (HRTEM-Titan G2). The spatial resolution of HRTEM was less than 0.15 at 300 kV. To conduct this experiment, the specimens (S1, S4, and S6) were prepared in the form of thin foil and thinned by the ion milling technique under the liquid nitrogen environment. The Fourier transformation of the diffraction profiles were also applied to obtain the curves of pair distribution function (PDF) for each sample. The details of TEM-based PDF analysis are given in Refs. [32,33]. To characterize the mechanical response of the amorphous specimens, the nanoindentation test was carried out at the room temperature under loading rate of 1 $\mathrm{mN\cdot s^{-1}}$. Moreover, the maximum load and the holding time at maximum load were 25 mN and 5 s, respectively. The 70 indents were analyzed for each situation to achieve reliable and precise results for the statistical evaluations. A Python script was composed for the automated detection pop-in events in the load-displacement curves. For counting and measuring the pop-in events reliably and precisely, the identification method was designed in accordance with the sudden indenting depth alterations. For this purpose, the displacement was calculated through the function of the square root of the load to obtain the linear format of parabolic load–displacement curves.[34] Afterwards, the derivative was evaluated with consideration of loading portions occurred in the nanoindentation results. It is worth-mentioning that a Savitzky–Golay filter was applied to decrease the influence of noise and improve the stability of analysis.[35] Moreover, a fitting line was employed to correct the derivative results, leading to a suitable baseline for the selection of pop-in events from the load-displacement curves with different slopes. Furthermore, the Vickers hardness of specimens was evaluated with a loading force 700 grf (1 grf = 635.460 μN) and a holding time of 5 s. The loading force was selected low enough to avoid any full penetration in the samples. The scanning electron microscopy (SEM-TESCAN Vega2) was used to observe the morphology of indenting area.

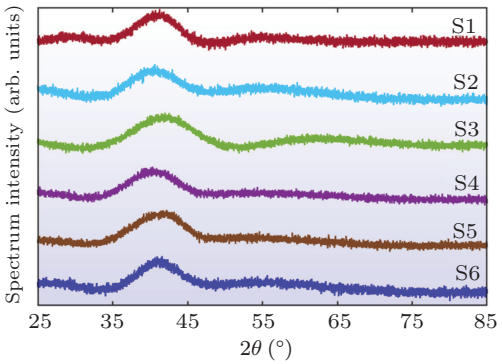


Fig. 1. X-ray diffraction curves of samples in different states.

3. Results and discussion

Figure 2 illustrates the DSC curves of all the samples in a wide range of temperature from the relaxation region up to the

melting temperature. Considering the $Fe_{80}P_{13}C_7$ alloy, it can be seen that the reduced glass transition, *i.e.*, T_{rg} (T_g/T_l), and the extent of super-cooled liquid region, *i.e.*, $\Delta T_x = T_x - T_g$, are respectively 0.527 and 29 K, which indicates the relatively low glass forming ability (GFA) in this alloying composition (see Table 1). Moreover, it is detected that the crystallization peak is divided into the two separated events, implying the formation of competitive crystalline phases during the heating stage in the DSC experiment. In the sample S2, the Ni addition leads to a slight decrease in T_g, T_x, and T_l; however, the values of T_{rg} and ΔT_x indicate a moderate increment. In general, it is believed that the mean bonding strength of atomic constitutes in an alloying system considerably affects T_x and T_g.[36,37] It is also suggested that the Ni constitute creates atomic pairs with smaller negative heat of mixing leading to the weakening of average bonding strength and the reduction of characteristic temperatures.[21,26,38] Moreover, the DSC curve of $Fe_{75}Ni_5P_{13}C_7$ alloy shows that the crystallization region and the melting transition stage happen in a narrower range of temperature without forming two-step events, compared with sample S1. This result reveals that the Ni-added alloy has a chemical composition near the eutectic composition. With the addition of Co into the base alloy (S3), the thermal behavior of amorphous ribbon changes significantly, so that the crystallization stage is divided into the three apparent peaks, which means that the compositional heterogeneity is intensified in the microstructure. Furthermore, one can see that the T_l value markedly decreases, while there is no significant alteration in T_x or T_g, compared with the base alloy (S1). In a study done by Xu *et al.*,[24] it was unveiled that the 5% Co addition increases the critical casting thickness in Fe–P–C system, which is consistent with our study indicating the improved T_{rg} value in the $Fe_{75}Co_5P_{13}C_7$ (S3). The thermal behavior of sample S3 can be also described by this fact that Co addition leads to the creation of chemical short range orders in the form of Fe_3Co type clusters inducing the variety of crystallization events during the heating process.[26]

Table 1. Temperature parameters extracted from the DSC results.

	S1	S2	S3	S4	S5	S6
T_g (K)	679	664	673	651	663	678
T_x (K)	708	697	704	689	689	712
T_l (K)	1288	1227	1185	1115	1156	1219
ΔT_x (K)	29	33	31	38	36	34
T_{rg}	0.527	0.541	0.567	0.583	0.573	0.556

When the Ni and Co elements are simultaneously increased into the system (S4), the thermal peaks of amorphous ribbon become similar to the $Fe_{80}P_{13}C_7$ composition, so that the crystallization event includes two distinguished peaks. Moreover, T_g, T_x, and T_l values are substantially declined and the GFA indicators, *i.e.*, T_{rg} and ΔT_x, are improved in the sample S4. This result indicated that the amorphous alloy gains the advantages of Co and Ni addition altogether in a way that the compositional heterogeneity and total heat of mixing reach an optimal value in the system. The 1-at.% and 5-at.% Cu were also added into the FeNiCoPC alloy to figure out whether the thermal features and the GFA improve in the system. The DSC results indicated that the 1-at.% Cu addition (S5) leads to a slight decrease in T_{rg} and ΔT_x values, while the glass formation properties of alloy significantly decrease when 5% Cu is added into the system (S6). This can be due to the fact that the Cu microalloying process leads to the deterioration of total negative heat of mixing in the alloying composition,[16] which is a detrimental factor for the glass formation possibility in the amorphous alloy.

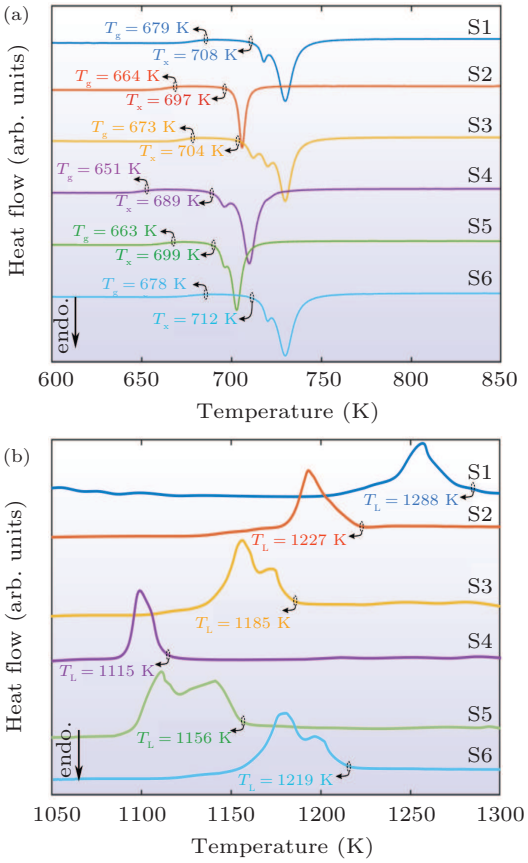


Fig. 2. DSC curves of samples at (a) relaxation–crystallization region, (b) liquidus region.

Figure 3 demonstrates the hysteresis M–H loops of all the samples defined by the vibrating sample magnetometer In this experiment, the density of samples was measured by the Archimedes's technique and the saturation polarization (J_s) was then calculated through the equation "$J_s = 4\pi \times 10^{-7}\rho M_s$" (Ref. [16]). Using this equation, it is possible to identify the maximum magnetic moment per unit volume for a magnetic material, which is a key parameter in the soft magnetic applications. At the first glance, one can see that the minor addition of elements plays the crucial role in magnetic

properties of Fe-based alloys, so that an extensive range of J_s is achieved in the experiment. Moreover, the mean magnetic moment value ($\bar{\mu}$), as the indicator of average magnetic strength in the alloying system with a specific magnetic field, shows a trend similar to the J_s values. For the sample S1, it is observed that the values of J_s and $\bar{\mu}$ yield 151.32 emu/g and 1.73 μ_B, respectively. The $\bar{\mu}$ value for this sample is lower than the pure Fe system with 2.2 μ_B, in which the magnetically inert p–d covalent pairs are replaced by the polarizable d–d bonds.[26,39] For the sample S2, the Ni addition decreases the J_s and $\bar{\mu}$ values to 147.05 emu/g and 1.681 μ_B, respectively. It is believed that the decrement is attributed to the dilution impact of Ni atoms on the total $\bar{\mu}$ of the alloying system.[26] Although, it is suggested that the Ni constitute acts as a paramagnetic factor in the base alloy, some studies indicated that the Fe–P–C system confronted a slight increment of Fe moment under the Ni addition.[11,23] This hypothesis covers our results, in which the sample S2 just exhibited a modest decline of J_s and $\bar{\mu}$. Considering the sample S3, one can observe that the magnetic properties of Fe-based alloy is improved through the minor addition of Co element, so that the J_s and $\bar{\mu}$ values reach 152.971 emu/g and 1.765 μ_B. In general, the F–P–C amorphous alloys include in the classification of ferromagnets, which implies the location of Fermi level at the valley of down-spin 3d band.[28,40] This event leads to the generation of holes on the spin band and the magnetization weakening in the alloying system. Under the Co minor addition, the Fe up-spin band gets involved by the electrons and a consecutive shift of half-bands happens through the Coulomb interactions.[41] As a result, the minor Co addition provides condition for improving the ferromagnetic properties of base alloy. The sample S4 exhibited the J_s and $\bar{\mu}$ values of 151.11 emu/g and 1.714 μ_B, implying that the Ni addition may undo the effects of Co microalloying on the magnetic properties of base alloy. Nevertheless, one can notice that the added Ni yields a slight decrement in the trend of μ, so that the J_s value remains in the range of base alloy (S1). The Cu microalloying also influenced the magnetic properties of Fe-based alloy; however, it is found that the impact degree strongly relies on the added concentration. The results indicate that the increase of Cu content from 1 at.% to 5 at.% leads to the sharp decrement of J_s from 150.98 emu/g to 147.34 emu/g. It is suggested that the extra addition of Cu leads to the decrement of ferromagnetic Fe content in the alloying system. moreover, it is believed that the increase in Cu content intensifies the total positive heat of mixing in the system, which leads to the rise of nanoscale structural heterogeneity.[16] This event induces the internal stresses in the atomic configuration and deteriorates the magnetic properties of MGs. Nevertheless, it should be noted that the higher structural heterogeneity induces more loosely packed structure in the alloy and provides more potential sites for creation of shear events in the glassy structure. The possibility of this phenomenon will be evaluated under the nanoindentation and HRTEM experiments. Moreover, it is worth-mentioning that other factors in the production of Fe-based alloys can improve the final magnetic properties. To provide some examples, many efforts have been made through the oxide fluxing treatment and the nanocrystallization process to promote the soft magnetic properties.[17,42–44] However, in this work, it was our aim to tune the comprehensive features of Fe-based alloy without manipulating the monolithic amorphous phase.

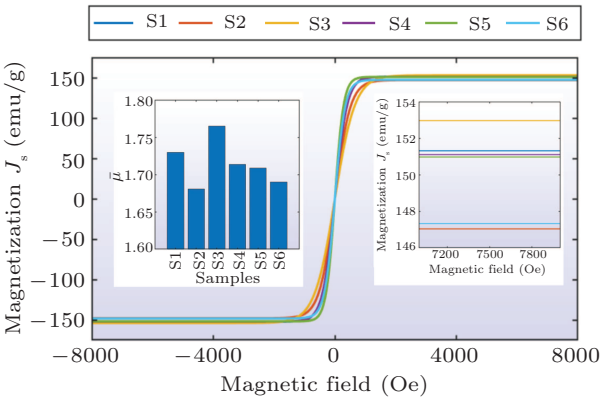


Fig. 3. Hysteresis curves of the specimens. The insets indicate the mean magnetic moment values and upright saturation zone. The unit 1 Oe = 79.5775 A/m.

The load–displacement curves of Fe-based amorphous alloys are given in Fig. 4(a). The results indicated that the addition of elements into the base alloy (S1) leads to the increment of displacement; however, its variation depends on the type of added elements. The magnified image from the displacement at the maximum load shows that the elemental addition also enhances the viscoplastic response of Fe-based alloy, so that the creep displacement reaches 26 nm in the $Fe_{65}Co_5Ni_5Cu_5P_{13}C_7$ (S6), which is 2.5 times higher than the sample S1 (see Fig. 4(b)). For detailed evaluation, the maximum displacement (d_{max}) and the final displacement (d_f) were considered as the significant parameters to identify the deformability of Fe-based alloys, as marked in Fig. 4(a). With comparison of the d_{max} and d_f values, it is possible to find out the level of anelastic strain in the Fe-based alloys, which is indicator of loosely packed regions in the glassy structure.[45] The d_f/d_{max} ratio in the amorphous alloys reflects the level of anelasticity in the microstructure (see Fig. 4(c)). With the addition of Ni and Co into the alloying system (S2, S3, and S4), the d_f/d_{max} ratio decreases, which means that the induced anelastic strain slightly declines, compared to the base alloy (S1). On the other side, the Cu addition (S5 and S6) leads to a

moderate increment, which indicates that more atomic movement occurs in an anelastic mode under the nanoindentation test. It is also concluded that there exists no direct correlation between the viscoplastic strain, manifested at the maximum load, and the anelastic strain energy. To evaluate the plastic behavior of Fe-based alloys, the magnitude of derivative $(\mathrm{d}h/\mathrm{d}F^{0.5})$,[34] which is indicative of alterations in the pop-in events and the force (F) variation, is calculated and plotted. As given in Fig. 5(a), the larger derivatives are signs of bigger pop-ins, while the smaller ones tend to have a lower derivative. The results also show that the samples S5 and S6 have the most contracted data with the lowest derivatives and the smallest pop-in events (see Fig. 5(a)), which means that the Cu addition plays an important role in the improvement of multiple shear banding events under an external excitation.[16] As illustrated in Fig. 5(b), the density of data is also altered with the change of chemical compositions. To provide some examples, the pop-in sizes in the sample S1 are distributed from 0 nm–6 nm; whereas, the size distribution of shear events in the sample S5 is limited to the range of 0 nm–3 nm. This result clearly indicates that the minor addition enhances the possibility of multiple shear banding events with small sizes, leading to a more homogenous plasticity in the MG. As a general assumption, the percolation of nanoscale shear transformation zones (STZs) is responsible for the creation and propagation of micro-scale shear banding events in the glassy structures.[46–48] In an amorphous material with the multiple shear events and lower derivatives (S5 and S6), the structural heterogeneity and loosely packed regions are intensified and the shear events are activated and propagated in a multiple mode, leading to an improved plasticity in the structure.

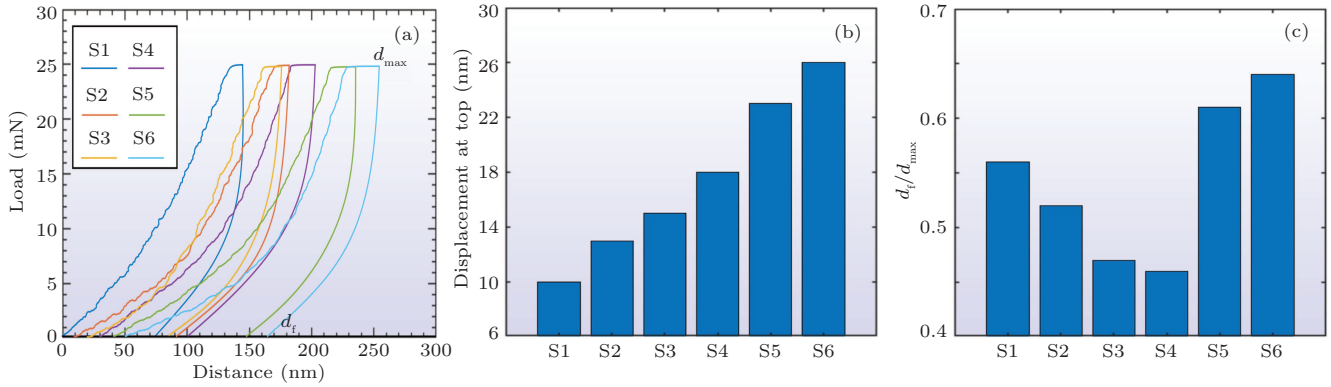


Fig. 4. (a) Load–displacement curves of samples under nano-indentation test, (b) creep displacement of samples at the top of curves, (c) d_f/d_{max} ratio measured from the curves.

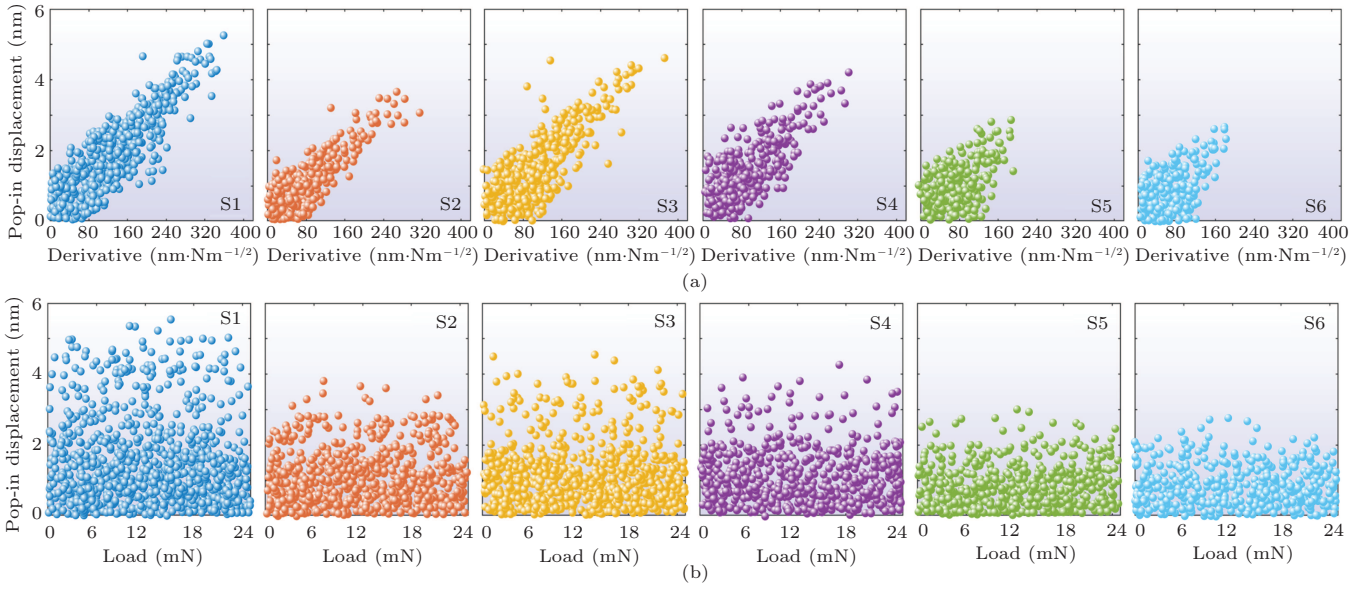


Fig. 5. Pop-in displacements as the function of (a) pop-in derivatives and (b) indenting load.

Figure 6(a) shows the SEM image of Vickers indenting area for the samples S1, S4 and S6. As observed, no obvious shear banding was occurred around the indenting area of sample S1. On the other side, the addition of Co/Ni (S4) into the alloying composition leads to the appearance of arc-shaped ripple signs adjacent to the indenting area. These signs are indicators of shear bands with a circle configuration, created during the indenting process. With the addition of Cu into the

alloying composition (S6), the population of shear bands increases around the indenting area and the width of shear events is extended. This indicates that the Cu addition intensifies the softening phenomenon in the MG structure. To better understand the role of Cu addition on the plasticity of our Fe-based MG, it is necessary to evaluate the atomic arrangements in the system. The analysis of atomic-scale arrangements of MGs provides important information regarding the structural evolution. For this purpose, the fast Fourier transformation of HRTEM images was obtained and the calculation of atomic density function was carried out. To resolve the inelastic scattering noises, the zero-loss energy filtering was applied. Moreover, a noise removing technique was used to smooth the PDF curves of samples. Figure 6(c) represents the PDF analysis of samples S1, S4, and S6. As observed, the first peak is located at the range of 2.6 nm–2.9 nm, which indicates the intensification of short range orders (SROs) in the alloys. Furthermore, the second peak at the range of 4 nm–5.8 nm introduces the level of atomic-cluster interconnection, which is identified as the medium range order.[49] The results indicated that the minor addition of Co/Ni (S4) leads to a slight weakening of SRO and MRO peaks in the PDF curve, which implies that the loosely packed structure gradually increases in the system. On the other side, one can see that the Cu addition (S6) not only declines the intensity of SRO and MRO peaks, but also widens the MRO peak and shifts it to the higher values. This result determines that the Cu addition increases the loosely packed structure in the system and also changes the interconnection of atomic clusters in the structure. When the MRO peak shifts to the higher values, the interpenetrating clusters disappear and the loosely connected arrangements are dominated at the nanoscale.[50] Consequently, the potential regions for creating and percolating of STZs enhances in the system, leading to the multiple fine shear banding under the indenting process (see Fig. 5).

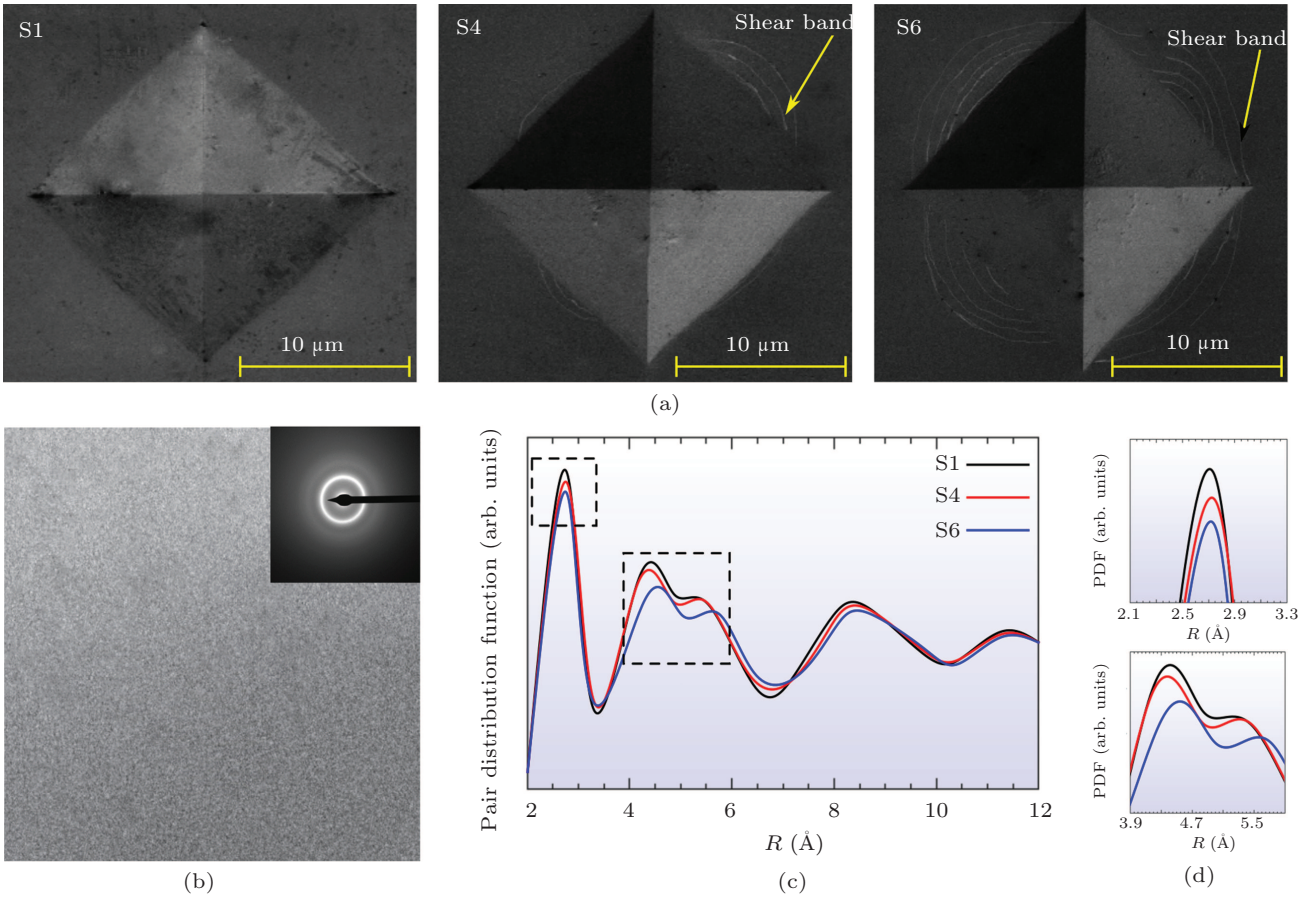


Fig. 6. (a) Vickers indenting area and the marked shear events in samples S1, S4, and S6; (b) TEM image and diffraction profile of sample S1; (c) PDF analysis of samples S1, S4, and S6; (d) magnified image of SRO and MRO peaks.

Figure 7 shows the variations of T_{rg}, ΔT_x, J_s, viscoplastic (Max. load displacement) and anelastic (d_f/d_{max}) indicators for all the samples. As observed, to obtain an engineering Fe-based amorphous alloy with satisfying comprehensive properties, it is required to have an optimization between the thermal, magnetic and mechanical features According to the results, the Cu addition into the FeNiCoPC system leads to the significant improvement in the plasticity, which is related to the enhancement of loosely packed regions and flow units.[17] However, this event comes at the expense of GFA and magnetic properties, which means that the high-concentrated Cu addition is not beneficial for the optimized properties. When the Cu

addition increases in the system, compositional heterogeneity enhances in the structure, which is led by the distribution of loosely packed regions.[16,17] This phenomenon intensifies the internal stresses in the structure, which may be harmful for the magnetic properties.[51] As marked in Fig. 7, 1-at.% Cu addition can improve the plasticity in the Fe–P–C-based alloy without significant decline in the GFA and J_s. On the other side, the simultaneous addition of Co and Ni makes an optimization in the glass formation and saturation magnetization. Consequently, it is believed that the suitable minor addition of elements, *i.e.*, Ni, Fe, and Cu, can tune comprehensive properties of Fe–P–C-based amorphous alloys without deteriorating any individual feature. In this work, the results suggest that the $Fe_{69}Co_5Ni_5Cu_1P_{13}C_7$ amorphous alloy exhibited the optimized state among the samples, so that the plasticity, glass formation, thermal stability and magnetic properties are acceptable for the engineering applications.

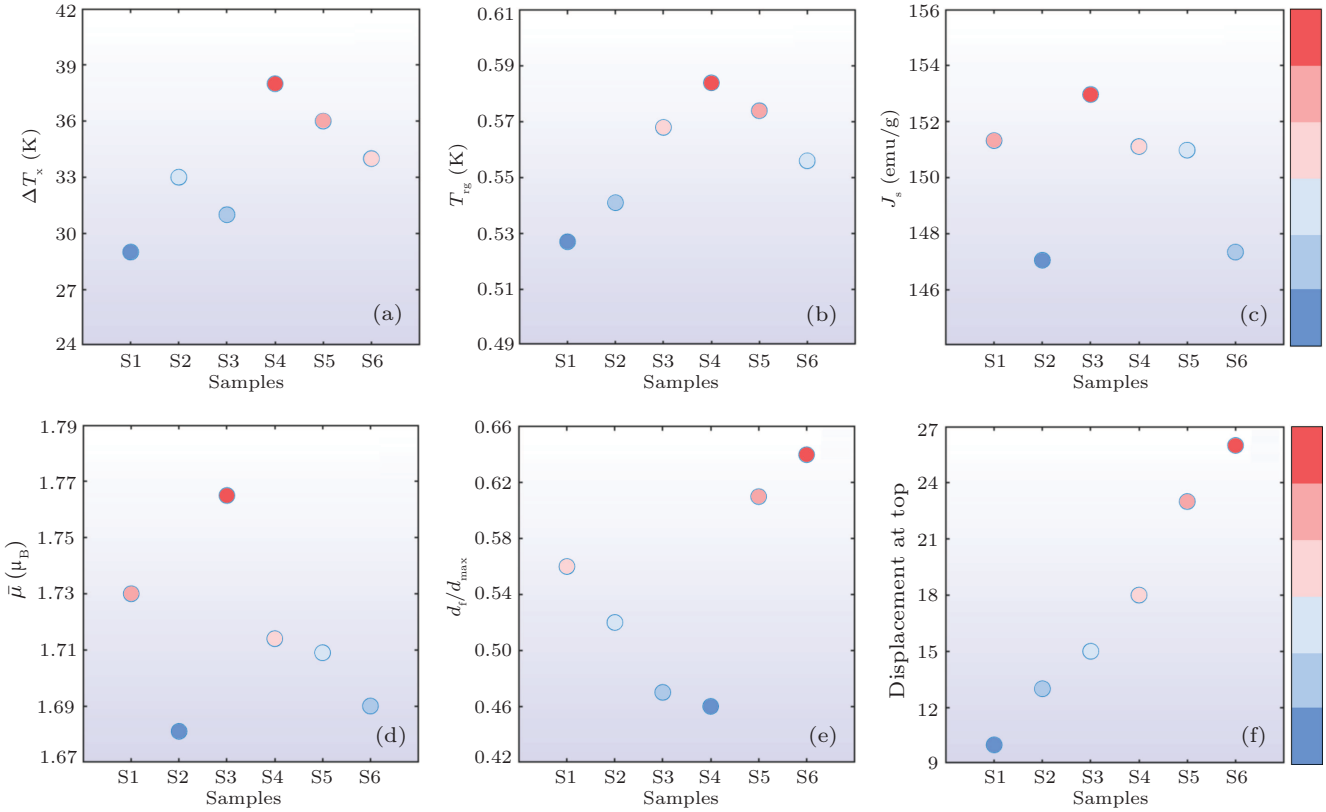


Fig. 7. The plotted values of (a) ΔT_x, (b) T_{rg}, (c) J_s, (d) $\bar{\mu}$, (e) anelasticity (d_f/d_{max}), (f) viscoplasticity (displacement at the top of nanoindentation curves). The colors show the intensification value of each indicator among the samples.

4. Conclusion

In this study, the Fe–P–C-based amorphous system was developed by the minor addition of Ni, Co and Cu constitutes. The main purpose of microalloying was to tune the comprehensive properties of the Fe–P–C-based alloy for the potential applications. The main outcomes of this work are as follows.

(i) The simultaneous minor addition of Co and Ni into the basic system leads to the maximum improvement of GFA and thermal stability. This promotion leads to the creation of near-eutectic composition and the generation of compositional heterogeneity, caused by the Ni and Co elements, respectively.

(ii) The sole Co addition plays the most important role in optimizing of J_s and $\bar{\mu}$ values; however, the minor addition of Ni and Cu elements slightly decreases the magnetic properties.

(iii) The best deformation behavior with high anelastic–viscoplastic properties is associated to the Cu-alloyed system, which is manifested in the appearance of small pop-in events with low derivatives along with the large displacement at the maximum load under the nanoindentation test. In summary, it was revealed that the $Fe_{69}Co_5Ni_5Cu_1P_{13}C_7$ alloying composition exhibited an optimized state for achieving the comprehensive properties.

References

[1] Sarac B, Ivanov Y P, Chuvilin A, Sch?berl T, Stoica M, Zhang Z and Eckert J 2018 *Nat. Commun.* **9** 1333
[2] Yang W, Huo J, Liu H, Li J, Song L, Li Q, Xue L, Shen B and Inoue A 2016 *J. Alloys Compd.* **684** 29
[3] Li Y, Lv K, Shen N, Chen X, Chen L, Li F and Hui X 2021 *J. Magn. Magn. Mater.* **530** 167915
[4] Stoica M 2017 *Fe-Based Bulk Metallic Glasses* (Springer)
[5] Azuma D, Ito N and Ohta M 2020 *J. Magn. Magn. Mater.* **501** 166373
[6] Suryanarayana C and Inoue A 2013 *Int. Mater. Rev.* **58** 131
[7] Sarker P C, Guo Y, Lu H Y and Zhu J G 2020 *J. Magn. Magn. Mater.* **514** 167290

[8] Zhou S X, Dong B S, Qin J Y, Li D R, Pan S P, Bian X F and Li Z B 2012 *J. Appl. Phys.* **112** 23514

[9] Yang W, Wang Q, Ling H, Liu H, Xue L, He Y, Li Q and Shen B 2019 *J. Alloys Compd.* **773** 401

[10] Wang Y, Xu K and Li Q 2012 *J. Alloys Compd.* **540** 6

[11] Yang W, Liu H, Zhao Y, Inoue A, Jiang K, Huo J, Ling H, Li Q and Shen B 2014 *Sci. Rep.* **4** 6233

[12] Meng S, Ling H, Li Q and Zhang J 2014 *Scr. Mater.* **81** 24

[13] Li W, Yang Y H, Xie C X, Yang Y Z, Liu H Y, Wang K W and Liao Z L 2020 *J. Magn. Magn. Mater.* **498** 166128

[14] Tjahjono T, Elveny M, Ibrahim O adil, Suharno, Chupradit S, Bokov D, Hoi H T and Pandey M 2021 *Trans. Indian Inst. Met.*

[15] Li J F, Liu X, Zhao S F, Ding H Y and Yao K F 2015 *J. Magn. Magn. Mater.* **386** 107

[16] Yang X, Wang T, Li Q, Wu R, Gao B and Yang Q 2020 *J. Non-Cryst. Solids* **546** 120274

[17] Hou L, Yang W, Luo Q, Fan X, Liu H and Shen B 2020 *J. Non-Cryst. Solids* **530** 119800

[18] Zhu L, Meng Y, Zhai X B, Wang Y G and Lan S 2019 *J. Magn. Magn. Mater.* **472** 49

[19] Shi Z, Li R, Li X, Wang C and Zhang T 2019 *Mater. Sci. Eng. A* **766** 138385

[20] Yang X, Ma X, Li Q and Guo S 2013 *J. Alloys Compd.* **554** 446

[21] Ma X, Yang X, Li Q and Guo S 2013 *J. Alloys Compd.* **577** 345

[22] Wan C, Yang W, Liu H, Zuo M, Li Q, Ma Z, Zhao Y and Inoue A 2018 *Mater. Sci. Technol.* **34** 751

[23] Liu Q, Liu H, Wang M, Zhang Y, Ma Z, Zhao Y and Yang W 2017 *J. Non-Cryst. Solids* **463** 68

[24] Xu K, Ling H, Li Q, Li J, Yao K and Guo S 2014 *Intermetallics* **51** 53

[25] Wang Y, Zhai H, Li Q, Liu J, Fan J, Li Y and Zhou X 2019 *Acta* **675** 107

[26] Y uce E, Sarac B, Ketov S, Reissner M and Eckert J 2021 *J. Alloys Compd.* **872** 159620

[27] Wang Q, Zhou J, Zeng Q, Zhang G, Yin K, Liang T, Yang W, Stoica M, Sun L and Shen B 2020 *Materialia* **9** 100561

[28] Shi Z, Li R and Zhang T 2019 *J. Alloys Compd.* **778** 302

[29] Bahrani S 2021 *Adv. Appl. NanoBio-Technologies* **2** 34

[30] Bakhshkandi R and Ghoranneviss M 2019 *J. Res. Sci. Eng. Technol.* **7** 1

[31] Samavatian M, Gholamipour R and Samavatian V 2021 *Comput. Mater. Sci.* **186** 110025

[32] Gorelik T E, Neder R, Terban M W, Lee Z, Mu X, Jung C, Jacob T and Kaiser U 2019 *Acta Crystallogr. Sect. B Struct. Sci. Cryst. Eng. Mater.* **75** 532

[33] Ketov S V, Trifonov A S, Ivanov Y P, Churyumov A Y, Lubenchenko A V, Batrakov A A, Jiang J, Louzguine-Luzgin D V, Eckert J, Orava J and Greer A L 2018 *NPG Asia Mater.* **10** 137

[34] Ebner C, Pauly S, Eckert J and Rentenberger C 2020 *Mater. Sci. Eng. A* **773** 138848

[35] Savitzky A and Golay M J E 1964 *Anal. Chem.* **36** 1627

[36] Chen H S 1980 *Rep. Prog. Phys.* **43** 353

[37] Wu Z W, Li M Z, Wang W H and Liu K X 2015 *Nat. Commun.* **6** 6035

[38] Anafcheh M 2021 *J. Appl. Org. Chem.* **2** 125

[39] Hafner J, Tegze M and Becker C 1994 *Phys. Rev. B* **49** 285

[40] Egami T 1984 *Rep. Prog. Phys.* **47** 1601

[41] Díaz-Ortiz A, Drautz R, Fähnle M, Dosch H and Sanchez J M 2006 *Phys. Rev. B* **73** 224208

[42] Shi L, Wang K and Yao K 2020 *J. Non-Cryst. Solids* **528** 119710

[43] Wu Y, Sun L, Li X, Shao P, Song K, Wang S, Wang L and Zhou S 2021 *J. Magn. Magn. Mater.* **528** 167825

[44] Shi L and Yao K 2020 *Mater. Des.* **189** 108511

[45] Shayakhmetov Y, Vorobeva A, Burlankov S, Bogonosov K, Fomin A, Goncharov A, Krasnikov S, Nikolaeva S, Ovsyannikova A and Zekiy A O 2021 *Mater. Res.* **24**

[46] Pan J, Ivanov Y P, Zhou W H, Li Y and Greer A L 2020 *Nature* **578** 559

[47] Qu R T, Wu S J, Wang S G, Wang X D and Zhang Z F 2020 *J. Mech. Phys. Solids* **138** 103922

[48] Liu Z, Huang P and Wang F 2021 *J. Alloys Compd.* **865** 158993

[49] Feng S D, Chan K C, Zhao L, Pan S P, Qi L, Wang L M and Liu R P 2018 *Mater. Des.* **158** 248

[50] Samavatian M, Gholamipour R, Amadeh A A and Mirdamadi S 2019 *J. Non. Cryst. Solids* **506**

[51] Zheng H, Zhu L, Jiang S S, Wang Y G, Liu S N, Lan S and Chen F G 2020 *J. Alloys Compd.* **816** 152549